Experimental and numerical study of a 10MW TLP wind turbine in waves and wind

Pegalajar Jurado, Antonio Manuel; Hansen, Anders Mandrup; Laugesen, Robert; Mikkelsen, Robert Flemming; Borg, Michael; Kim, Taeseong; Heilskov, Nicolai F.; Bredmose, Henrik

Published in:
Journal of Physics: Conference Series (Online)

Link to article, DOI:
10.1088/1742-6596/753/9/092007

Publication date:
2016

Document Version
Publisher's PDF, also known as Version of record

Experimental and numerical study of a 10MW TLP wind turbine in waves and wind

2016 J. Phys.: Conf. Ser. 753 092007

(http://iopscience.iop.org/1742-6596/753/9/092007)

Experimental and numerical study of a 10MW TLP wind turbine in waves and wind

Antonio Pegalajar-Jurado[1], Anders M. Hansen[1], Robert Laugesen[1], Robert F. Mikkelsen[1], Michael Borg[1], Taeseong Kim[1], Nicolai F. Heilskov[2] and Henrik Bredmose[1]

[1] DTU Wind Energy, Nils Koppels Allé, Building 403, DK-2800 Kgs. Lyngby, Denmark
[2] DHI, Agern Allé 5, DK-2970 Hørsholm, Denmark

E-mail: ampj@dtu.dk

Abstract.

This paper presents tests on a 1:60 version of the DTU 10MW wind turbine mounted on a tension leg platform and their numerical reproduction. Both the experimental setup and the numerical model are Froude-scaled, and the dynamic response of the floating wind turbine to wind and waves is compared in terms of motion in the six degrees of freedom, nacelle acceleration and mooring line tension. The numerical model is implemented in the aero-elastic code *Flex5*, featuring the unsteady BEM method and the Morison equation for the modelling of aerodynamics and hydrodynamics, respectively. It was calibrated with the tests by matching key system features, namely the steady thrust curve and the decay tests in water. The calibrated model is used to reproduce the wind-wave climates in the laboratory, including regular and irregular waves, with and without wind. The model predictions are compared to the measured data, and a good agreement is found for surge and heave, while some discrepancies are observed for pitch, nacelle acceleration and line tension. The addition of wind generally improves the agreement with test results. The aerodynamic damping is identified in both tests and simulations. Finally, the sources of the discrepancies are discussed and some improvements in the numerical model are suggested in order to obtain a better agreement with the experiments.

1. Introduction

The dynamic response of a floating wind turbine depends on several elements, such as the aerodynamic loads on the rotor, the hydrodynamic loads on the floater, the restoring effect of the mooring lines and the structural properties of the turbine and floater. Each of these elements enters into the general equations of motion and can be modelled with a simpler or more detailed approach. Therefore, there is a trade-off between model accuracy and computational cost. The accuracy of a numerical model can be assessed by comparing its performance to equivalent tests. While several models for floating wind turbines exist, their validation can hardly be made at full scale due to the limited number of turbines and the uncertainties in the environmental conditions. In the current study, we present an experimental test campaign of the 1:60 scaled DTU 10MW reference wind turbine [1] mounted on a tension leg platform (TLP), as detailed in [2] and [3]. The experimental campaign is part of the INNWIND.EU project [4]. The numerical model [5] is implemented in *Flex5* [6] in scale 1:60 as well [7]. The test results are analyzed with respect to response and aerodynamic damping, and the ability of the model to reproduce these phenomena is assessed. Finally, some improvements for the numerical model are suggested.

2. Experimental setup

The Froude number (Fr) is preserved in the scaling of the experimental setup [8][9]. The Reynolds number (Re), however, cannot be simultaneously preserved due to limitations in the test facility. Hence, the scaled rotor had to be redesigned to produce the right thrust, as detailed in [10] (see Fig. 1). The rotor design employs a selection of special low-Reynolds-number airfoils, namely *SD7003* ($t/c = 8.51\%$), *SD7032* ($t/c = 9.95\%$), *SD7062* ($t/c = 13.98\%$) and a circular profile ($t/c = 100\%$) from blade tip to root. The design preserves the tip-speed ratio (TSR) and results in a chord length increase of 75% relative to pure geometric scaling, in order to obtain the right scaled thrust. The associated angle of attack hereby defines the twist distribution of the blade.

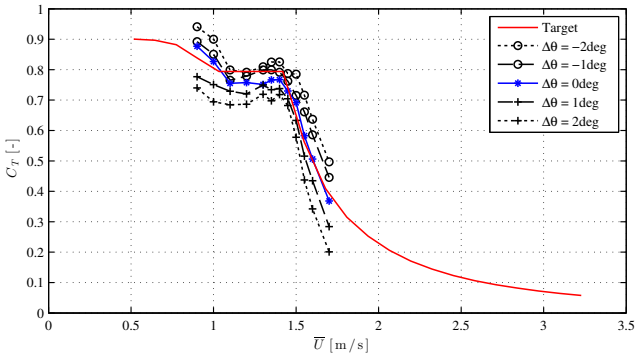

Figure 1: Experimental thrust coefficient C_T for different wind speeds $\bar{U}$. The DTU 10MW curve was matched in the tests by adding a calibrated $\Delta\theta$ to the reference blade pitch angle.

The TLP foundation was designed with *WAMIT*, using design information on TLP platforms in the offshore industry, as well as [11]. Details on the design can be found in [3]. Given the maximum wave in the 50-year, 3-hour storm, the floater submergence and the freeboard of the transition piece were chosen so that the floater top is below the wave trough and the connection between transition piece and wind turbine tower is above the wave crest. Likewise, the tendons were not allowed to have an angle with the vertical above 10 deg, and their tension limits were defined by zero — to avoid slack tendons — and twice the tension in the equilibrium position. Furthermore, attention was given to the coupled natural frequencies of the floating wind turbine, so they do not overlap with forcing frequencies such as the wave frequency range or the 1P and 3P frequency ranges for the rotor.

Sketches of the experimental setup at DHI Denmark are shown in Fig. 2. The wave basin is 20 m long, 30 m wide and 3 m deep, which corresponds to a water depth of 180 m in full scale. The wind generator, mounted on top of the wave maker, is 4 m by 4 m and can provide wind speeds up to 1.7 m/s, corresponding to 13.2 m/s in full scale. The TLP wind turbine was located 4 m downwind. The data acquisition system was located on the bridge (blue truss) and stored all the relevant data with a sampling frequency of 160 Hz, including: the free surface elevation, measured by 11 wave gauges at different locations (see Fig. 2(b)); the wind speed, measured with air velocity transducers at the TLP location before the experiments; the line tension in each of the mooring tendons, measured by Z-gauges; the shear force between nacelle and tower; the floater acceleration in three directions and the nacelle acceleration in fore-aft and side-side directions; and the motion of the floater in six degrees of freedom (surge, sway, heave, roll, pitch, yaw) obtained with a Qualisys system, which employs two infrared cameras and a number of reflective markers attached to the floater.

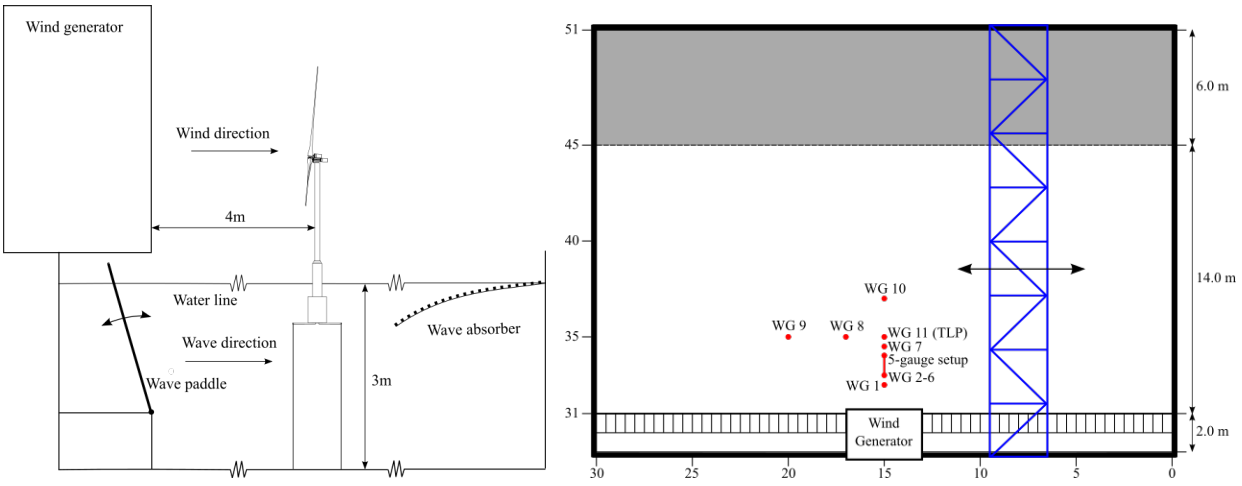

(a) Side view (b) Top view

Figure 2: The experimental setup.

In order to remove high-frequency components in the measured data that do not originate from a physical process, a low-pass Butterworth filter with a high-cut frequency of 8 Hz was applied to all test signals. In addition, for the tests with wind, it was observed that the heave, pitch and roll signals consistently presented a series of unphysical peaks. The presence of these peaks was attributed to the momentary loss of the position of one of the markers in the Qualisys system, due to the passing of a wind turbine blade. Hence, a median filter was applied to these three signals in the tests with wind in order to remove the undesired peaks. The median filter replaces every value in the signal with the median of a window centered at the mentioned point and a user-defined width, which for the present study was chosen to be 25 points.

3. Numerical setup

The numerical model used for the present study was based on an existing *Flex5* [6] implementation of a TLP wind turbine [5] available at DTU Wind Energy. The model features the unsteady Blade Element Momentum (BEM) method for the aerodynamic loads, and the wind field is based on the Mann model [12]. Under the assumption of a slender body, the hydrodynamic forcing is governed by the Morison equation and the viscous effects are solely accounted for through the Morison drag term. The model does not accommodate frequency-dependent hydrodynamic added mass or damping, nor user-defined linear damping. The hydrodynamic added mass matrix was taken as constant at the zero-frequency limit. The wave kinematics are computed with linear wave theory. Consistently with linear theory, the hydrodynamic forces are integrated up to Sea Water Level (SWL) at $z = 0$. This simplification does not have a significant impact on the hydrodynamic loads, as they are known to be inertia-dominated in the test regime.

Due to the choice of Froude-scaling, the Reynolds number is not preserved in the scaling process. Hence, for a given wind speed V the redesigned scaled rotor will generally produce a different mean thrust force T than the reference DTU 10MW wind turbine for the same operational conditions — rotor speed ω and blade pitch θ. We consider the thrust as the most important aerodynamic element in the overall dynamics of a floating wind turbine, therefore it is desirable to match the scaled thrust of the reference wind turbine for each wind speed. Both in the experimental setup and in the numerical model the steady thrust curve was matched to that of the DTU 10MW turbine by modifying the blade pitch settings for each wind speed until

the mean thrust was equal to the target (see Fig. 3). The rotor speed ω was always set to the downscaled reference curve.

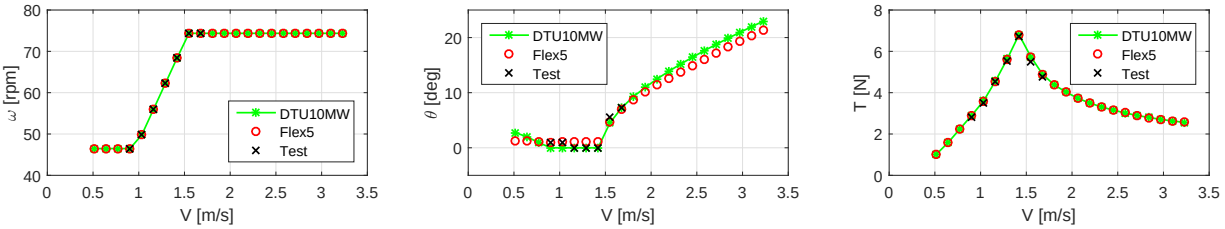

Figure 3: Matching of the thrust curve.

Further, the free decay surge response of the floating wind turbine observed in the tests was reproduced in the model by manually adjusting the hydrodynamic coefficients in the Morison equation. The added mass coefficient C_m was set to 0.765 in order to match the surge natural frequency of 0.19 Hz. The Morison drag coefficient C_D was first estimated as 1.5 for the surge decay test based on values of the Reynolds and Keulegan-Carpenter (KC) numbers [13]. Then it was observed that a value of $C_D = 1.7$ was necessary in order to match the damping ratio in the free decay test. Hence, an identical correction factor was applied to the drag coefficients previously estimated for each sea state. This approach was chosen as a pragmatic solution given the limitations of the model, although the addition of linear or quadratic damping would be a worthy alternative. The natural frequency of the TLP wind turbine in pitch was observed to be 1.9 Hz, hence the same natural frequency was obtained in the *Flex5* model by adjusting the tendon stiffness from $EA = 80$ kN (measured value) to 90 kN. Since the focus of the present study is on the in-plane motion of the TLP wind turbine (surge, heave, pitch), and given the absence of a heave decay test to compare to, no further tuning of the numerical model was carried out.

4. Environmental conditions

Once calibrated, the numerical model was used to reproduce the response of the TLP wind turbine to the same environmental conditions (EC) as in the tests (see Table 1, where the conditions EC1-EC7 are identical to those used in the first floating wind turbine test campaign [14] within *INNWIND.EU*). Since the maximum wind speed delivered by the wind generator was 1.7 m/s, the tests corresponding to EC6-EC10 were run with a wind speed of 1.7 m/s, and the wind turbine was operated accordingly. The turbulence intensity measured in the test facility was 5%, obtained from the time series of wind speed $V(t)$ as the ratio of standard deviation to mean value, $TI = \sigma_V/\bar{V}$. The wind fields used as input for the numerical model were produced as standard inflow fields with *IECTurbulenceSimulator*, with the same mean wind speed and turbulence intensity as the corresponding test. For each case, the wave elevation measured by the wave gauge WG8 (see Fig. 2 (b)) was used to compute the corresponding wave kinematics for the numerical model by linear wave theory. Due to limitations in the wave basin, it was not possible to generate the irregular sea states for EC9 and EC10.

5. Response to regular waves

The results for regular waves without wind corresponding to EC5 and EC10 can be seen in Fig. 4. A sample of the time series is shown for the response in surge ξ_1, heave ξ_3 and pitch ξ_5, as well as for the nacelle fore-aft acceleration a_{nac} and the mooring line tension. Given the alignment of

Table 1: Target environmental conditions for the tests, based on [15]. H_s is the significant wave height, T_p is the wave peak period and $\bar{U}$ is the 10-min averaged wind speed. The corresponding full-scale values are in parentheses.

	EC1	**EC2**	**EC3**	**EC4**	**EC5**	**EC6**	**EC7**	**EC8**	**EC9**	**EC10**
H_s [m]	0.039	0.047	0.055	0.062	0.069	0.103	0.130	0.167	0.200	0.239
	(2.34)	(2.82)	(3.30)	(3.72)	(4.14)	(6.18)	(7.80)	(10.02)	(12.00)	(14.34)
T_p [s]	0.71	0.78	0.84	0.89	0.94	1.15	1.29	1.58	1.76	1.99
	(5.50)	(6.04)	(6.51)	(6.89)	(7.28)	(8.91)	(9.99)	(12.24)	(13.63)	(15.41)
$\bar{U}$ [m/s]	0.9	1.0	1.1	1.3	1.5	2.3	3.2	4.3	5.2	6.2
	(7.0)	(7.7)	(8.5)	(10.1)	(11.6)	(17.8)	(24.8)	(33.3)	(40.3)	(48.0)

the TLP symmetry axis with the wind and wave direction for the cases considered in this study, the front line tension T_{front} is presented as the mean of the tension at the two front lines, and T_{back} is the mean tension at the back lines.

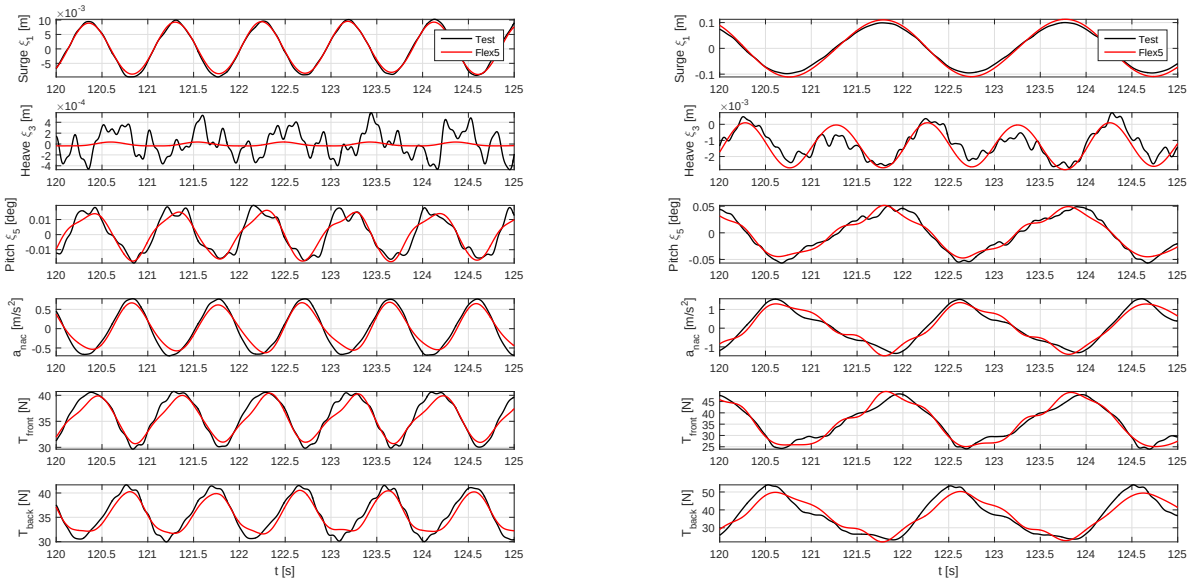

(a) EC5

(b) EC10

Figure 4: Response to regular waves.

From the time series in Fig. 4 it can be observed that there is a very good match in surge motion for EC5, while the agreement is not as good for EC10. Since EC10 corresponds to the largest wave, the induced motions will be largest and limitations of the linear wave forcing model are likely to affect the model accuracy. For heave, given the relatively small amplitude of the motion of a TLP foundation in this degree of freedom, the test signal is subjected to a high level of uncertainty — as seen for EC5, where positive heave values are clearly unphysical. However, a certain agreement is observed for EC10, where the surge motion — and consequently the heave motion, which is heavily coupled to the former — is largest. The test pitch signal is believed to

be amplified by a certain factor, likely due to an inadequate gain value in the data acquisition system. Unfortunately, the calibration factor for the logged platform pitch signal was lost after the test campaign. Given the fair agreement between tests and simulations in regular waves for surge, nacelle acceleration and line tension, it was decided to apply a linear recalibration by reducing the test pitch signal with a factor α for all cases. The value of α was sought so that the ratio of spectral peak $\hat{\xi}(f)$ in pitch and surge at the wave frequency f_p (i.e. $\hat{\xi}_5(f_p)/\hat{\xi}_1(f_p)$) was the same for *Flex5* and test. This approach would make the choice of α independent of the added mass coefficient C_m, which is a user-defined parameter in the model. The value α=7.3 was found by applying the mentioned procedure for two regular waves within the linear regime, EC5 and EC8. After the recalibration was applied, a fair agreement between test and simulation was found, although the model slightly underpredicts the peaks in pitch motion for EC5. This slight underprediction from the *Flex5* model is also translated into a smaller nacelle acceleration and line tension for EC5. However, for EC10, where the agreement in pitch is better, a closer match is also found for nacelle acceleration and line tension.

6. Response to irregular waves and wind

The results for irregular waves are presented for EC3 (Fig. 5), EC5 (Fig. 6) and EC7 (Fig. 7). In each plot the responses with and without wind are shown. Given the stochastic nature of the time series, a comparison in terms of exceedance probability is preferred in this case. For each individual wave in the time series of surface elevation, a time window is defined and the peak of each response signal within this window is stored. These peaks are then sorted from minimum to maximum, and an exceedance probability P_{exc} is assigned to them based on their position on the sorted list. Since the exceedance probability corresponds to the probability of a particular extreme value being exceeded, the lowest probabilities correspond to the most extreme peaks. However, line tension is a special case, where the probability analysis is applied twice. First, the minima in the signal are stored and sorted in descending order, which produces the left branch of the probability curves. Second, the maxima are seeked and sorted in ascending order, producing the right branch. The two branches are plotted together for convenience, hence the reason why these curves are not monotonous as is the case for the classical exceedance probability curves.

The *Flex5* surge motion without wind roughly agrees with the tests, although with a little underprediction, given that the test signal contains more energy at the surge natural frequency. The disagreement seems to grow with the sea state, which could be attributed to the increase in nonlinearity as the wave height grows larger. For all the cases considered in this study, the presence of wind — which offsets the structure from its equilibrium position — improved the match in surge motion. For combined wind and wave forcing a very good match in surge is seen.

The heave and surge motions in a TLP are coupled, so that the TLP describes the upper part of a circular trajectory in the surge-heave plane. Hence, without wind, the structure will oscillate around its equilibrium position, resulting in a very limited motion in heave and consequently in a significant level of uncertainty in the measured signal. This effect is observed for EC3 (Fig. 5), where there is a very poor match between tests and simulations, even when wind is included. However, larger surge motion occurs for larger sea states, which leads to larger heave motion through the coupling. Hence, larger waves will result in a better match in heave motion, as shown for EC7 (Fig. 7). On the other hand, the wind will displace the TLP from its equilibrium position, and the same surge amplitude will result in a larger heave amplitude. Thus, a good match in heave is expected for medium and large sea states with wind, as seen for EC5 and EC7.

The TLP is very stiff in pitch, hence a small range of pitch motion and a certain level of uncertainty is also expected for this degree of freedom. Larger sea states will cause a larger pitch

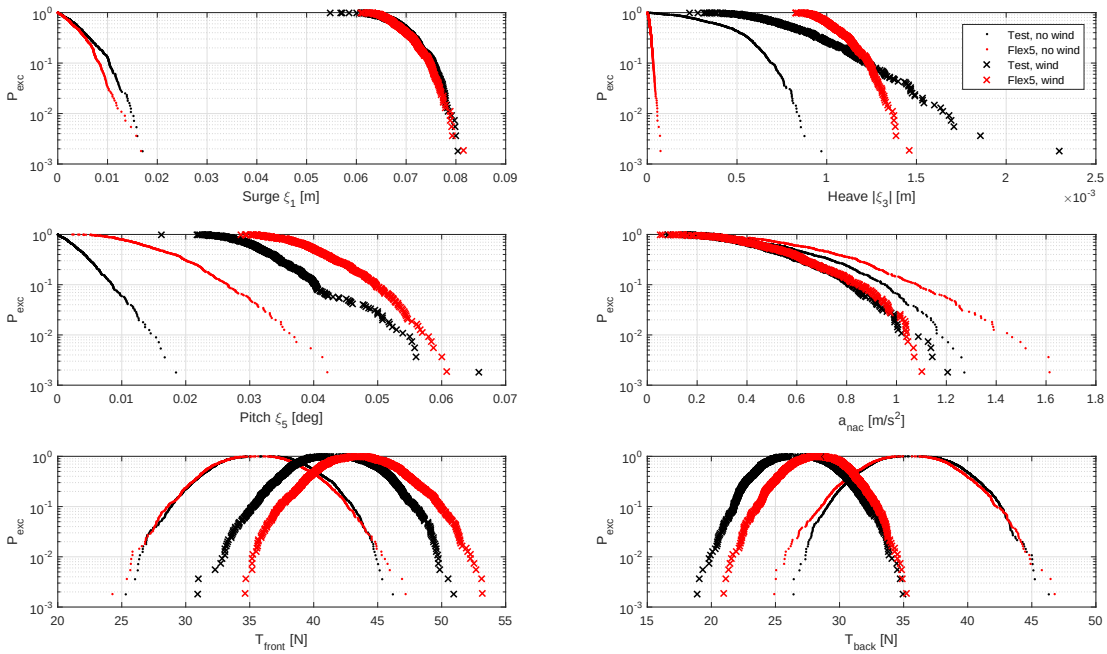

Figure 5: Response to irregular sea state EC3, with and without wind.

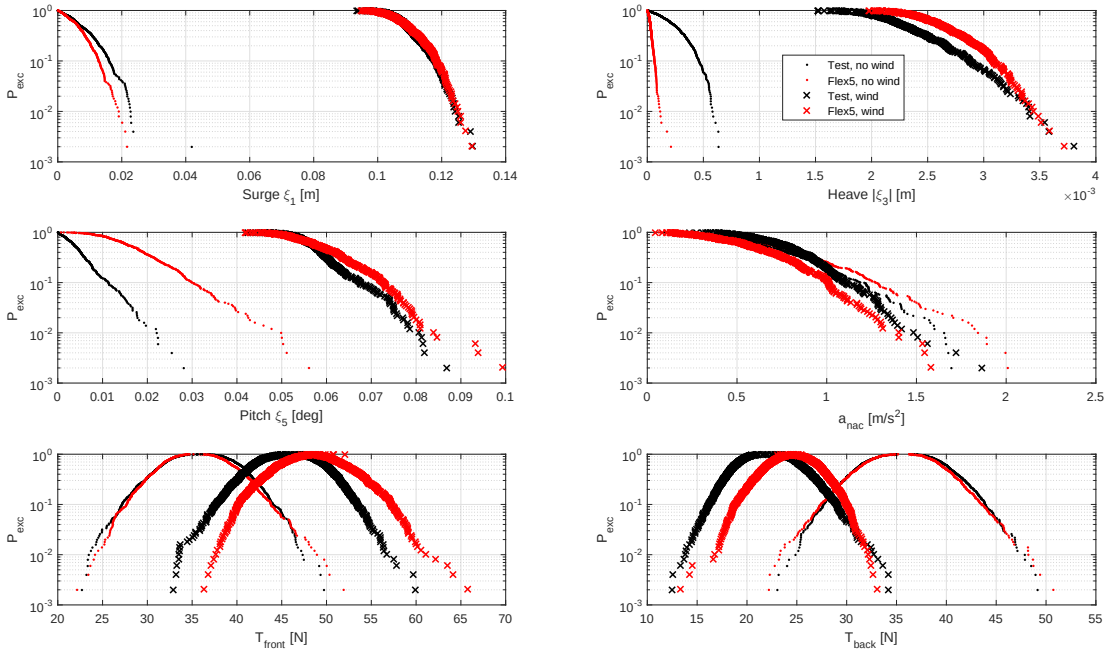

Figure 6: Response to irregular sea state EC5, with and without wind.

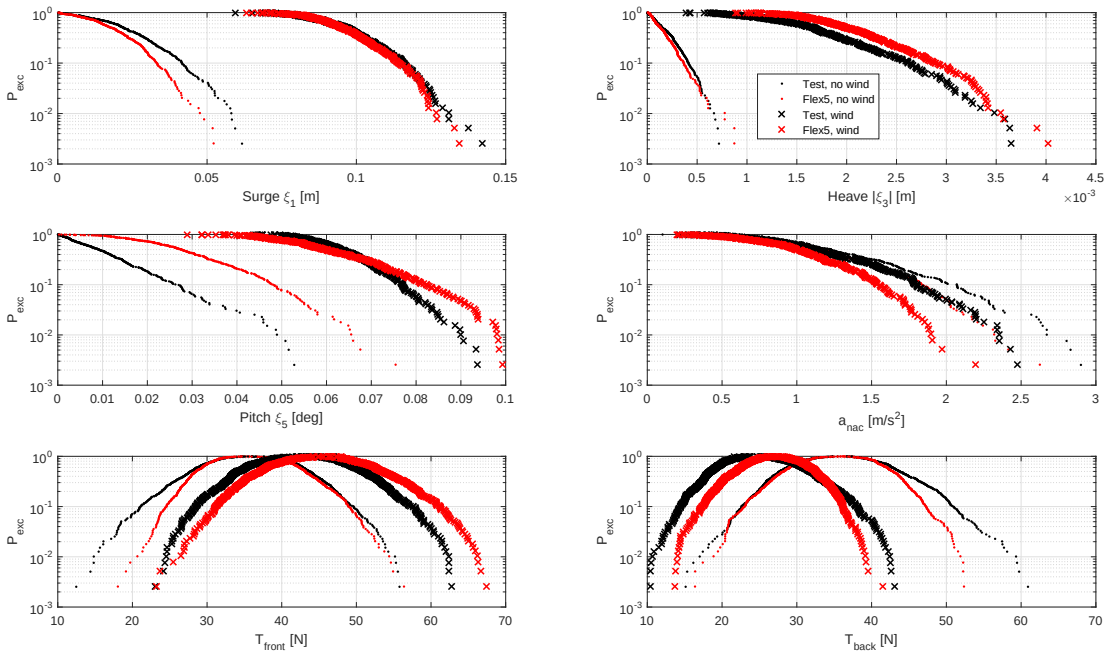

Figure 7: Response to irregular sea state EC7, with and without wind.

motion, bringing the test and simulation curves closer as the sea state grows. However, the pitch motion without wind was systematically overpredicted by *Flex5*, as the motion contain more energy at the pitch natural frequency than the signal of the corresponding tests. The wind also introduces an offset in platform pitch and improves the match between tests and simulations, as seen especially for EC5 and EC7.

Obtaining a good match in nacelle fore-aft acceleration represents a bigger challenge, since it depends on surge, pitch and tower deflection. However, the predictions are in general acceptable, particularly for EC5 (rated wind speed). The nacelle acceleration was also used to investigate the effect of aerodynamic damping on the structure. It is well known that the thrust force is proportional to the square of the relative wind speed and to the angle of attack seen by the blades. Hence, when the rotor is moving towards the wind, a larger relative wind speed is seen and a larger thrust force is experienced. The opposite phenomenon takes place when the rotor moves with the wind. This effect is known as aerodynamic damping and reduces the amplitude of the nacelle motion when wind is present. For the three EC shown here, it is observed that the nacelle acceleration is always reduced when compared to the same case without wind, hence proving that the effect of aerodynamic damping is visible both in the experiments and the numerical results. It was desirable to quantify the amount of aerodynamic damping, but the extraction of such quantity for a case with irregular waves is not straight-forward. Hence, a surge decay scenario with and without wind was selected for this purpose. It was found that the wind at rated wind speed introduces an additional damping ratio in the surge decay signal of ξ=2.9% in *Flex5* and 6.8% in the tests. Both the model and the experiment show the effect of damping. The disagreement in the quantified damping can be related to the difference between the test wind field and the wind input for *Flex5*.

The match in line tension is also acceptable in most of the cases. In general, the pitch motion has the largest impact on the tendon elongation, hence some correlation is expected between both. A correlation can be found between the overpredicted pitch motion and the larger front tension in *Flex5*, especially in cases with wind. The mean displacement in surge and pitch introduced by the wind increases the loading on the front tendons and relieves the back tendons. This effect is visible here for both tests and simulations, as a shift to the right in the front tension and a shift to the left in the back tension.

To further investigate the effect of wind on the response, the corresponding signals were separated into mean $\bar{x}$ and deviation from the mean Δx, such that every signal $x(t)$ could be expressed as $x(t) = \bar{x} + \Delta x(t)$. The effect of wind on the mean values for all sea states is shown in Fig. 8, where nacelle acceleration is not applicable. The uncertainty in heave and pitch for EC1 is too large in the tests, hence these two signals are not to be taken into account in EC1. EC5 corresponds to rated wind speed, while EC6 and EC7 operate under the same wind speed (maximum in generator, 1.7 m/s) and EC8 corresponds to a storm condition with parked turbine. The plot shows an increase of mean surge and heave with the sea state, reaching the maximum at rated wind speed and decreasing afterwards. This is consistent with the thrust curve (Fig. 3, right) which shows that the maximum thrust — and therefore the maximum offset in surge and heave — occurs at rated wind speed. The pitch motion in *Flex5* also follows this behaviour. However, the pitch in the tests presents a second peak for EC7, which corresponds to the same wind speed as EC6 but a more severe sea state. This observation could be attributed to the absence of mean drift forces in the numerical model. This perception is consistent with EC8 as well, where the turbine is parked — hence the loads are mainly wave-induced — and a much larger mean pitch is observed in the test. Consistently with the mean displacement introduced by the wind, the front line tension also increases up to rated wind speed and decreases afterwards, while the back line tension presents the opposite behaviour.

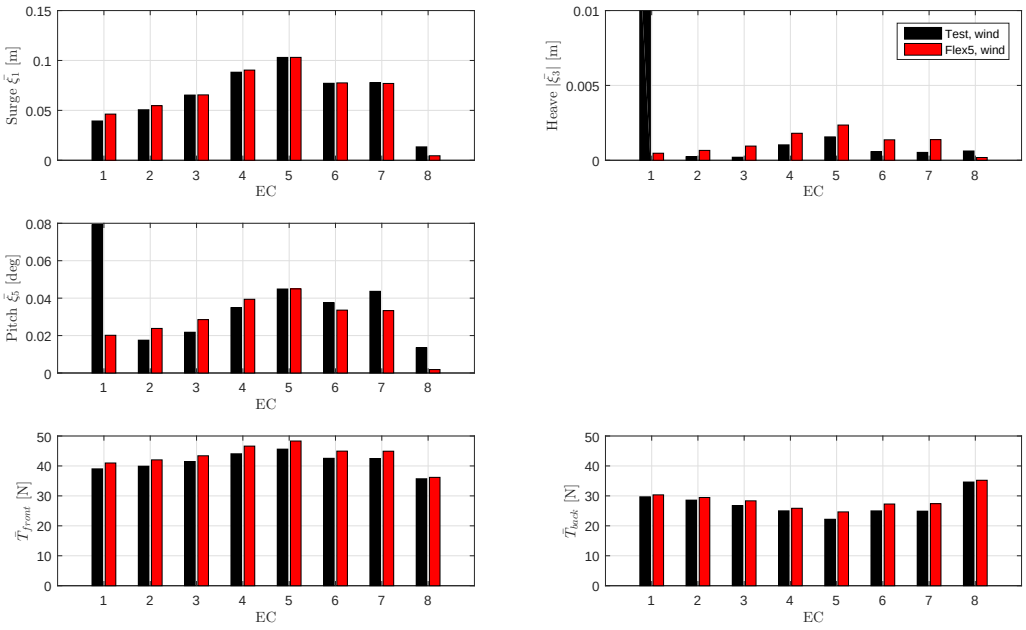

Figure 8: Effect of wind on the mean values for all EC.

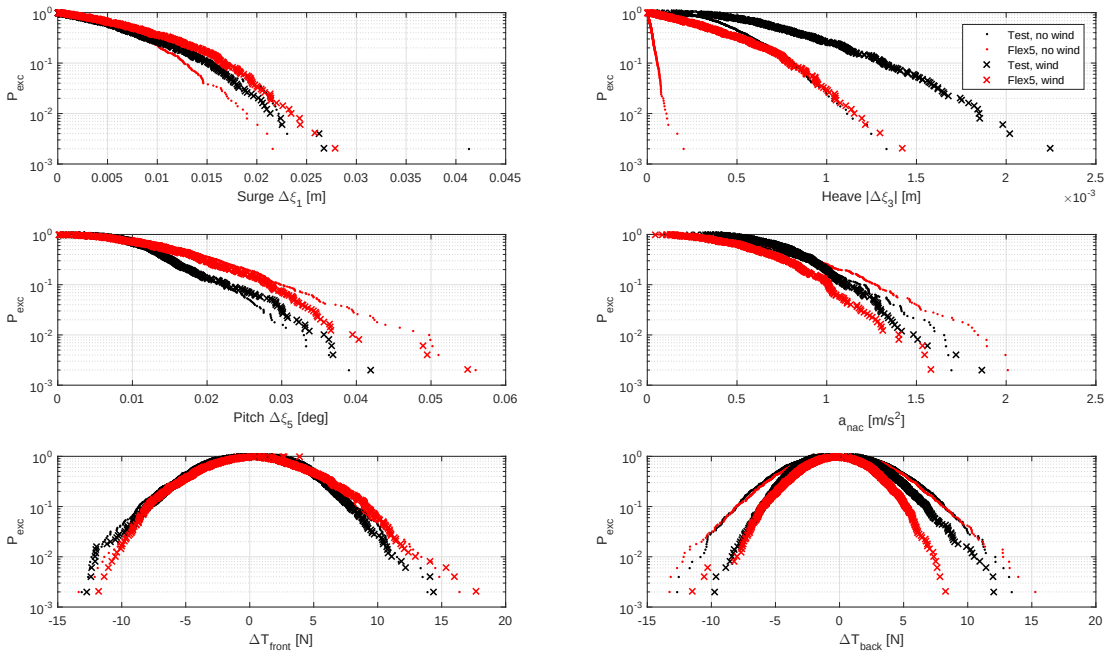

Figure 9: Effect of wind on the deviation from the mean values for EC5 (rated wind speed).

Fig. 9 shows the response to EC5, but now the mean has been subtracted from all signals in order to assess the effect of wind on the deviation from the mean. In surge, the wind slightly reduces the amplitude of surge motion in the tests, while the numerical model shows the opposite behaviour. The heave amplitude is enhanced due to wind for both model and test, as expected. The pitch motion is amplified by the wind in the test, while reduced by it in the simulation. However, although the effect of wind on surge and pitch is the opposite for tests and simulations, they both agree on a reduction of the nacelle acceleration due to wind, as stated previously. For the most extreme values, the wind increases the amplitude of the tension in the front tendons and reduces it for the back tendons, although the effect is much more visible for the latter. This behaviour is observed in both experiment and numerical model.

While the effect of wind on the mean of the signals is well reproduced by the numerical model, some of the dynamic effects show different behaviour between test and numerical prediction. One obvious mechanism that can explain that is the difference in the dynamic properties of the wind field — open jet in the test facility versus free atmosphere in the model.

7. Conclusions

A study of the numerical predictions compared to the tests was conducted, and results in surge were found to agree between tests and simulations. Even in extreme sea states, a good match in surge was obtained after calibration. The heave motion presents a certain correlation for the intermediate sea states, while for the smaller ones the measurements were too influenced by uncertainty. For the larger sea states, as well as for intermediate sea states with wind, a reasonable match with the test signal was found. The measured pitch response was proven to be unrealistic, thus a linear recalibration of the signal was needed to compare it to the predictions. Even after recalibration, significant discrepancies between tests and simulations were found for pitch with only waves — likely due to a larger amount of energy at the pitch natural frequency

in *Flex5* — while a closer match is obtained for the cases with wind and waves. The nacelle acceleration did not match as well as the motion signals did for all cases, but the aerodynamic damping was observed in both experimental and numerical setup. The line tension is generally well predicted, although in some cases the numerical model underpredicts the extreme loads.

A number of improvements need to be implemented in the model in order to enhance its reliability. These improvements include: the modelling of the TLP flexible spokes, which would influence the hydrodynamics and the structural response; a more detailed modelling of the hydrodynamics by introducing frequency-dependent added mass and radiation damping, as well as second-order effects such as mean drift forces; the inclusion of non-linear wave kinematics as an input for the model; and a more advanced computation of the wind field that ressembles better the actual wind conditions in the test facility.

To summarize, the present study analyzes the physical results of the experimental campaign, and proves the ability of the mentioned numerical model to reproduce the response of the TLP wind turbine to wind and waves with a certain level of confidence.

Acknowledgements
This work is part of the project INNWIND.EU [4]. The research leading to these results has received funding from the European Community's 7th Framework Programme under grant agreement No. 308974.

References
[1] Bak C, Zahle F, Bitsche R, Kim T, Yde A, Henriksen LC, Andersen PB, Natarajan A, Hansen MH. Description of the DTU 10 MW Reference Wind Turbine. DTU Wind Energy Report-I-0092. Roskilde, Denmark, 2013.
[2] Bredmose H, Mikkelsen RF, Hansen AM, Laugesen R, Heilskov N, Jensen B, Kirkegaard J. Experimental study of the DTU 10 MW wind turbine on a TLP floater in waves and wind. Presented at EWEA Offshore 2015 Conference. Copenhagen, Denmark, 2015.
[3] Hansen AM, Laugesen R. Experimental study of the dynamic response of the DTU 10MW wind turbine on a tension leg platform. MSc thesis, DTU Wind Energy. Kgs. Lyngby, Denmark, 2015.
[4] INNWIND.EU project. *URL: http://www.innwind.eu.*
[5] Ramachandran, GKV. A numerical model for a floating TLP wind turbine. PhD thesis, DTU Wind Energy. Kgs. Lyngby, Denmark, 2013.
[6] Øye S. FLEX4 simulation of wind turbine dynamics. *Proc. 28th IEA meeting of experts concerning state of the art of aero-elastic codes for wind turbine calculation*, 1996.
[7] Pegalajar-Jurado A. Numerical reproduction of laboratory experiments for a TLP wind turbine. MSc thesis, DTU Wind Energy. Kgs. Lyngby, Denmark, 2015.
[8] Martin HR, Kimball RW, Viselli AM, Goupee AJ. Methodology for wind/wave basin testing of floating offshore wind turbines. *Proc. 31st International Conference on Ocean, Offshore and Arctic Engineering.* Rio de Janeiro, Brazil, 2012. p. 10-15.
[9] Bredmose H, Larsen SE, Matha D, Rettenmeier A, Marino E, Saettran L. D2.4: Collation of offshore wind-wave dynamics. Technical report, Marine Renewables Infrastructure Network (MARINET). 2012.
[10] Mikkelsen RF. The DTU 10MW 1:60 model scale wind turbine blade. Technical report. Kgs. Lyngby, Denmark, 2015.
[11] Bachynski, EE. Design and dynamic analysis of tension leg platform wind turbines. PhD thesis, Norwegian University of Science and Technology. Trondheim, Norway, 2014.
[12] Mann J. Wind field simulation. *Problems in Engineering Mechanics*, vol.13, 1998. p.269-282.
[13] Sumer BM, Fredsøe J. *Hydrodynamics around cylindrical structures* (Singapore: World Scientific Publishing Co. Pte. Ltd.), 2006.
[14] Sandner F, Amann F, Azcona J, Munduate X, Bottasso CL, Campagnolo F, Robertson A. Model building and scaled testing of 5MW and 10MW semi-submersible floating wind turbines. Presented at EERA DeepWind 2015 Conference. Trondheim, Norway, 2015.
[15] Johannessen K, Meling TS, Haver S. Joint distribution for wind and waves in the northern North Sea. *Eleventh International Offshore and Polar Engineering Conference and Exhibition.* Stavanger, Norway, 2001.